Allosteric Activation of *Arabidopsis* Threonine Synthase by *S*-Adenosylmethionine

Gilles Curien,* Dominique Job, Roland Douce, and Renaud Dumas

Unité mixte CNRS/Rhône-Poulenc (UMR 41), Rhône-Poulenc Agrochimie, 14-20, rue Pierre Baizet, 69 263 Lyon Cedex 09, France

Received January 9, 1998; Revised Manuscript Received July 10, 1998

ABSTRACT: Plant threonine synthase, in contrast to its bacterial counterpart, is strongly stimulated by *S*-adenosylmethionine via a noncovalent interaction [Giovanelli et al. (1984) *Plant. Physiol. 76*, 285−292]. The mechanism of activation remained, however, largely unknown. To further characterize this unusual role for *S*-adenosylmethionine, the *Arabidopsis thaliana* threonine synthase was overexpressed in *Escherichia coli*, purified to homogeneity, and then used for kinetic and enzyme-bound pyridoxal 5′-phosphate fluorescence equilibrium-binding experiments. We observed that the activating effect of *S*-adenosylmethionine results from an 8-fold increase in the rate of catalysis and from a 25-fold decrease in the K_m value for the *O*-phosphohomoserine substrate. The data can be well fitted by a kinetic model assuming binding of two *S*-adenosylmethionine molecules on the native enzyme. We suggest that the dramatic modifications of the enzyme kinetic properties originate most presumably from an allosteric and cooperative transition induced by *S*-adenosylmethionine. This transition occurs at a much faster rate in the presence of the substrate than in its absence.

The aspartate derived amino acids pathway in plants has raised strong interests over the past few years when the inhibition of several enzymes in the pathway was proved to be herbicidal (*1*). More recently, the possibility of obtaining transgenic plants with increased levels of the essential amino acids methionine, lysine, and threonine (*2*) has contributed to stimulate researches on this metabolic pathway in plants. These agrochemical and nutritional applications require detailed studies of the enzyme kinetics and regulatory mechanisms. Our study of plant threonine synthase takes place in this context.

Plant threonine synthase (EC 4.2.99.2), a pyridoxal 5′-phosphate dependent enzyme, catalyzes the last step of threonine formation (*3*), converting *O*-phosphohomoserine (OPH)[1] to threonine and phosphate.

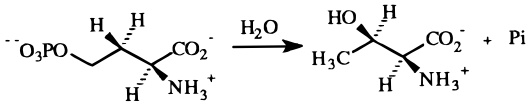

Threonine is directly incorporated into protein or further deaminated to yield oxobutyrate which serves as a precursor for isoleucine biosynthesis. In plant cells, OPH also serves as a precursor for methionine/*S*-adenosylmethionine (SAM) biosyntheses (Figure 1). Thus, threonine synthase competes for OPH with cystathionine-γ-synthase, the first committed enzyme in the methionine pathway (*4*). Flux coordination between threonine and methionine branches in plants does not result from end-product retroinhibition of the two enzymes. Indeed, no inhibition could be demonstrated for threonine synthase either by threonine or isoleucine (*4*) and for cystathionine-γ-synthase by either methionine or SAM (*5*). Instead, flux coordination appears to result in all plants so far tested via a strong stimulation of threonine synthase activity by SAM, the end-product of the methionine pathway (*3*, *5*−*8*). It is worth noting that, contrary to the plant enzyme, bacterial threonine synthase, though catalyzing the same reaction, is not subjected to kinetic modulation by SAM (*8*), most presumably because in bacteria OPH is not a branch point metabolite. Indeed, in prokaryotes, branching between threonine/isoleucine and methionine pathways occurs upstream of OPH, at the level of homoserine. Therefore, in bacteria a kinetic competition for OPH does not exist (*9*).

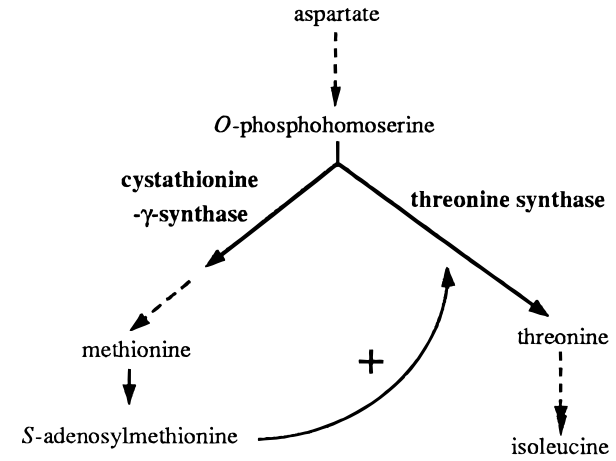

FIGURE 1: The threonine and methionine biosynthetic branches of the aspartate derived amino acids pathway in plants. *O*-phosphohomoserine is a branch point intermediate between methionine/*S*-adenosylmethionine and threonine/isoleucine pathways. *S*-adenosylmethionine acts as an allosteric activator of threonine synthase.

Apart from being a prerequisite for providing an integrated comprehension of the OPH flux partition, a detailed study of plant threonine synthase is of basic interest because of its

* Corresponding author. Fax: + 33 4 72 85 22 97.

[1] Abbreviations: DTT, dithiothreitol; OPH, *O*-phosphohomoserine; PLP, pyridoxal 5′-phosphate; SAM, *S*-adenosylmethionine.

S0006-2960(98)00068-3 CCC: $15.00
Published on Web 08/29/1998

noncovalent interaction with SAM. To our knowledge only one other enzyme, the mammalian cystathionine-β-synthase has been reported to be allosterically activated by SAM (*10*). Yet, the effector role of SAM in this new class of enzyme is totally unknown.

Previous kinetic data obtained with partially purified (about 40-fold) threonine synthase from pea (*7*) and from *Lemna* (*4*) suggested that the plant enzyme is highly specific for its substrate OPH and activator SAM. Evidence was also obtained suggesting that enzyme activity is stimulated in a sigmoidal and reversible manner by the activator (*4*). However, the kinetic mechanism of the enzyme-catalyzed reaction in the absence of SAM, as well as the mechanism of interaction between the enzyme and the activator, remains largely unknown due to the difficulty in obtaining large amounts of pure enzyme when starting from plant tissue.

To go further in the study of plant threonine synthase, the previously isolated cDNA encoding plastidial *Arabidopsis* threonine synthase (*8*) was used to overproduce the mature form of the *Arabidopsis thaliana* enzyme in *Escherichia coli* cells. To perform kinetic and equilibrium binding studies, the recombinant enzyme was then purified to apparent homogeneity. We demonstrate in the present paper that SAM activates plant threonine synthase by increasing both the rate of catalysis and the rate of OPH binding to the enzyme active site through a ligand-induced conformational change of the protein.

MATERIALS AND METHODS

Chemicals. OPH was synthesized as previously described (*11*). ^{1}H, ^{13}C, and ^{31}P NMR analyses showed that the OPH preparation was free of homoserine, inorganic phosphate, and adenine nucleotides. The OPH concentration of working solutions was determined after alkaline phosphatase treatment by determination of the amount of liberated inorganic phosphate (*12*). SAM (Boehringer) was purified by chromatography on a 1 $\times$ 5 cm^2 CM Sephadex (C25, Pharmacia) column (*13*) with elution in 50 mM HCl. The concentration of SAM was calculated using a molar extinction coefficient at 260 nm of 15 400 M^{-1} cm^{-1} (*14*).

Construction of the pKKTSmat Plasmid Encoding Mature A. thaliana Threonine Synthase. The pKKTSmat plasmid coding for mature *A. thaliana* threonine synthase was constructed via mutagenesis by PCR using the pYESTS3 threonine synthase cDNA as a template (*8*). This cDNA contains the entire sequence of mature threonine synthase minus the first Thr codon. The PCR fragment corresponding to the mature threonine synthase sequence was synthesized by using the following 5′-phosphorylated oligonucleotides: P1 (5′−CATGGCCGATGGCAACAACATCAAAGCC-3′) which introduced the ATG translation−initiation codon (underlined) in place of the codon corresponding to the first residue of the mature protein (Thr); P2 (5′-CAAACTTTGCGATAGAACTTTATTGGAAAAC-3′) which is complementary to the 3′ noncoding region of the cDNA downstream from the stop codon. PCR was conducted on 250 ng of template for 19 cycles including 1 min denaturation at 95 °C, 1 min of hybridization at 55 °C, and 2 min of DNA elongation driven by the proofreading *Pwo* DNA polymerase (Boehringer) at 72 °C. PCR blunt-ended generated fragments were subcloned into the pKK 223-3 vector (Pharmacia) digested by *Eco*RI and treated with Klenow DNA polymerase I. Ligation product was used to transform electrocompetent *E. coli* JM 105 bacteria. When correctly oriented, the threonine synthase cDNA is under the control of pTAC promoter.

Expression and Purification of Recombinant Threonine Synthase. E. coli JM 105 cells transformed with pKKTSmat plasmid were grown at 37 °C in Luria broth supplemented with pyridoxine (10 μM), thiamin (15 μM), and carbenicillin (100 μg/mL) until A_{600} reached 0.6. Thiamin is required because pyridoxine inhibits endogenous thiamin biosynthesis (*15*). Expression of the recombinant protein was induced by addition of 1 mM isopropyl β-D-thiogalactopyranoside, and the culture was continued at 37 °C for 16 h. Cells from a 2 L culture were harvested by centrifugation at 2000*g* for 15 min and resuspended in buffer A (50 mM Na−Hepes, pH 7.5, 1 mM EDTA, 1 mM DTT) containing protease inhibitors (5 mM ϵ-aminocaproic acid and 1 mM benzamidine). Cells were then disrupted by sonication for 10 min at 0 °C, and lysates were centrifuged at 28000*g* for 20 min. The supernatant was supplemented with 0.1% (w/v) streptomycin sulfate, and the solution was stirred for 15 min at 4 °C. Following centrifugation at 28000*g* for 30 min, the pellet was discarded and the supernatant (1.3 g protein, 30 mL) was applied onto a Fractogel DEAE EMD 650 (M) column (2.6 $\times$ 30 cm^2) equilibrated in buffer A. Proteins were eluted with a linear gradient of NaCl (0−300 mM in 400 mL of buffer A). Threonine synthase activity was eluted at a concentration of 250 mM NaCl. Active fractions (89 mg of protein) were concentrated on Macrosep 30 K (Filtron), desalted on a PD 10 column (Pharmacia) equilibrated in buffer A, and then applied onto a Resource Q column (1.5 $\times$ 15 cm^2) equilibrated in buffer A. Proteins were eluted with a linear gradient of NaCl (0−300 mM in 300 mL of buffer A). Threonine synthase activity was eluted at 250 mM NaCl. Pure threonine synthase (11 mg) was concentrated on Macrosep 30 K (Filtron) and desalted on a PD 10 column (Pharmacia) equilibrated in 20 mM Na−Hepes, pH 7.5. The enzyme was frozen in liquid nitrogen and stored in 20 mM Na−Hepes, pH 7.5, at −80 °C for months without any loss of activity. N-terminal sequence was verified for the purified recombinant threonine synthase with a model 494 gas−liquid-phase protein sequencer (Applied Biosystems). Furthermore, the lysine residue involved in PLP binding to the enzyme was determined as previously described (*16*) by sequencing the purified PLP-containing peptide.

Native Molecular Mass Determination. Gel filtration experiments were conducted on a Superdex 200 column (Pharmacia) in 50 mM Na−Hepes, pH 7.5, 150 mM NaCl, either in the absence or presence of 500 μM SAM.

Electrophoresis and Protein Determination. SDS/PAGE was performed according to Chua (*17*). Protein was measured either by the method of Bradford (*18*) using the Bio-Rad protein assay reagent with bovine γ-globulin as the standard or by measuring A_{205} (*19*). Concentration of homogeneous threonine synthase was calculated on the basis of a subunit molecular mass of 53 700 (*8*).

Threonine Synthase Assay. Threonine synthase activity was measured in a volume of 100 μL containing 50 mM Na−Hepes, pH 8.0, in the presence of appropriate concentra-

Table 1: Purification of Recombinant *A. thaliana* Chloroplastic Threonine Synthase Overproduced in *E. coli*[a]

purification stage	total protein (mg)	total activity (μmol of threonine formed/min)	specific activity (activity/mg of protein)	yield (%)
crude extract of soluble proteins	1300	260	0.2	100
EMD DEAE 650 (M) pool	89	151	1.7	58
resource Q pool	11	43	3.8	16

[a] Protein in the crude extract was determined with the Bio-Rad protein assay (Bradford method) with γ-globulin as the standard. Protein from the last two steps was determined from the absorbance at 205 nm. Enzyme activity was measured in 50 mM Na−Hepes pH 8.0 buffer with 1 mM OPH and 100 μM SAM.

tions of OPH substrate and SAM activator. Assays were initiated by adding enzyme (0.5−10 μg, corresponding to a concentration of 0.1−1.8 μM on a per subunit basis). After incubation at 30 °C for 20 s to 10 min, reactions were stopped by addition of 10 μL of 20% TCA. Threonine formation was quantitated by HPLC as previously described (*8*).

Spectroscopic Determinations. Absorption spectra of threonine synthase were recorded in a 1 cm optical-path-length quartz cuvette (200 μL) using an Uvikon 860 (Kontron) spectrophotometer thermostated at 30 °C. Fluorescence spectra were recorded with a SFM25 (Kontron) fluorimeter, using a 1 cm optical-path-length quartz cuvette (200 μL). An excitation wavelength of 410 nm was used to monitor fluorescence emission from the PLP cofactor of threonine synthase. The binding of SAM to the free enzyme was measured through the variations of the emitted fluorescence of enzyme (489 nm) upon SAM addition. Absorption and fluorescence assays were carried out in a 200 μL solution containing 50 mM Na−Hepes, pH 8.0, 150 mM NaCl, and 2 μM enzyme subunit.

Determination of the Stoichiometry PLP/Subunit. Protein was denatured in 0.1 M NaOH. This treatment shifted the absorption maxima for bound PLP to 390 nm, which corresponds to the absorption maxima for free PLP in solution (*20*). From absorbance measurements, concentrations of tyrosine (ϵ_{280nm} =1875 M^{-1} cm^{-1}, $\epsilon_{294.4nm}$ = 2850 M^{-1} cm^{-1}), tryptophan (ϵ_{280nm} = 6790 M^{-1} cm^{-1}, $\epsilon_{294.4nm}$ = 2855 M^{-1} cm^{-1}), and PLP (ϵ_{280nm} = 1120 M^{-1} cm^{-1}, $\epsilon_{294.4nm}$ = 1042.8 M^{-1} cm^{-1}, ϵ_{390nm} = 7680 M^{-1} cm^{-1}) of the protein solution were determined. Since the number of tryptophan and tyrosine residues in the primary sequence of the protein is known (*8*), the subunit concentration can then be estimated and compared with the PLP concentration determined.

Kinetic Data Analyses. Kinetic data were fitted to the appropriate theoretical equations by using the KaleidaGraph program (Abelbeck software) and a Macintosh Performa 475 computer.

RESULTS

Purification of Mature Recombinant Threonine Synthase and Spectral Properties. The enzyme was purified from *E. coli* JM 105 transformed with a plasmid (pKKTSmat) containing a cDNA for *A. thaliana* mature threonine synthase (i.e., without its plastidial transit peptide). The two-step purification procedure described under Materials and Methods resulted in an overall 20-fold purification with a yield of enzyme activity of about 16% (Table 1), and 11 mg of pure mature threonine synthase was obtained from 2 L of cell culture (Figure 2). N-terminal sequencing gave a single sequence of 10 amino acid residues (ADGNNIKAPI),

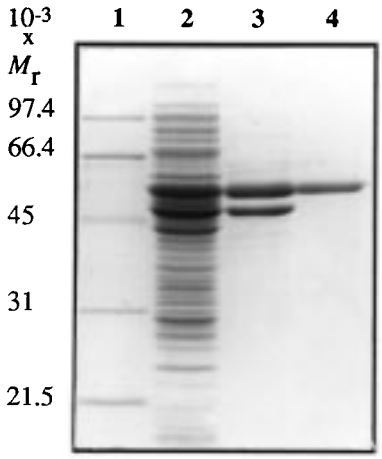

FIGURE 2: SDS/PAGE analysis of threonine synthase from *A. thaliana* at various steps of purification from overproducing *E. coli* cells. Proteins were separated on a 12% (w/v) polyacrylamide slab gel under denaturing conditions and stained with Coomassie Brilliant Blue R 250. Lane 1, M_r markers; lane 2, soluble proteins of the *E. coli* crude extract, 50 μg; lane 3, EMD DEAE 650 (M) pool, 6 μg; lane 4, Resource Q pool, 3 μg (see Table 1).

indicating that the initiating methionine inserted in place of the threonine residue in *A. thaliana* threonine synthase (*8*) was cleaved in the recombinant enzyme.

The native enzyme purified from *A. thaliana* is a homodimer of M_r 110 000 (*8*). Gel-filtration experiments were conducted with the recombinant native enzyme in the presence or absence of 500 μM SAM. In both cases, an apparent molecular mass of 110 000 corresponding to a homodimer was calculated thus indicating that SAM does not modify the oligomerization state of the dimeric threonine synthase.

The absorption spectrum of the purified threonine synthase at pH 8.0 exhibited maxima at 330 and at 410 nm besides the protein absorption at 280 nm. Since the maxima at 330 and 410 nm were found to be pH dependent (not shown), they can be assigned to the unprotonated (330 nm) and protonated (410 nm) forms of the Schiff base formed between PLP and a lysine residue in the protein (*21*). This residue was biochemically determined (see Materials and Methods) and assigned to Lys-202 in the sequence of *A. thaliana* threonine synthase (8). Absorbance measurements indicated a stoichiometric ratio between PLP and enzyme subunit.

Steady-State Kinetics. Under the experimental conditions of Materials and Methods, product formation was linear with time (Figure 3) at any OPH substrate and activator SAM concentration, testifying adherence to steady-state conditions. These steady-state rates were independent of the order of addition of substrate, SAM, or enzyme. Linearity was also observed in the absence or in the presence of SAM when measured as a function of protein concentration. The

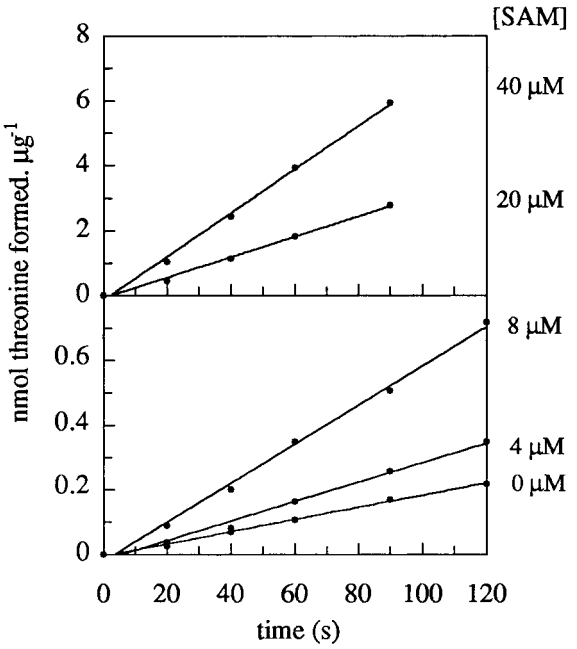

FIGURE 3: Threonine production as a function of time. Threonine formation was followed as a function of time in the presence of 50 μM OPH substrate and SAM activator at the concentrations indicated in the figure. Reactions were initiated by addition of the enzyme to the preincubated reaction mix. An enzyme subunit concentration of 0.4 μM was used for measurements in the presence of 0, 4, and 8 μM SAM and of 0.04 μM in the presence of 20 and 40 μM SAM. Straight lines were calculated by linear regression analysis. Mean correlation coefficient for the whole data in Figure 3: $r^2 = (0.9952 \pm 0.0026)$.

influence of SAM on enzyme activity was assessed by determination of k_{cat} and apparent K_m^{OPH} values as a function of SAM concentration. When the concentration of OPH was varied in the range 0−3 mM at fixed concentrations of SAM (from 0 to 60 μM), curves shown in Figure 4A were obtained. All curves fit well with a hyperbolic function (eq 1), thus revealing a Michaelis−Menten behavior with respect to the substrate at any SAM concentration.

$$\frac{v}{[E]_0} = k_{cat}\frac{[OPH]}{K_m^{OPH} + [OPH]} \quad (1)$$

where v represents the steady-state velocity, $[E]_0$ the total enzyme concentration, and k_{cat} the catalytic constant. An examination of the data in Figure 4A indicates, however, that SAM strongly affected both the rate of the enzyme-catalyzed production of threonine (k_{cat}) and the K_m^{OPH} value.

The influence of SAM on the catalytic constant (k_{cat}) was determined in the presence of a saturating concentration (5 mM) of OPH. As Figure 4B shows, SAM considerably increased k_{cat} from a value of 0.4 s^{-1} in the absence of SAM to a value of 3.5 s^{-1} at 60 μM SAM. Figure 4B also shows that k_{cat} increased in a sigmoidal fashion with SAM concentration.

From Figure 4A, K_m^{OPH} values were calculated and plotted as a function of activator concentration. As Figure 4C shows, SAM affected the K_m^{OPH} value in a complex fashion. In the 0−2 μM SAM concentration range, the K_m^{OPH} value abruptly increased from 250 to 500 μM. Then, above 2 μM SAM, this value strongly decreased with increasing SAM concentration. Half decrease in the K_m^{OPH} value was obtained at about 10 μM SAM. At 60 μM SAM, K_m^{OPH} reached a value of 10 μM, corresponding to a 25-fold decrease compared to the value in the absence of SAM and to a 40-fold decrease compared to the value in the presence of 2 μM SAM. Above 60 μM SAM, the K_m^{OPH} value still

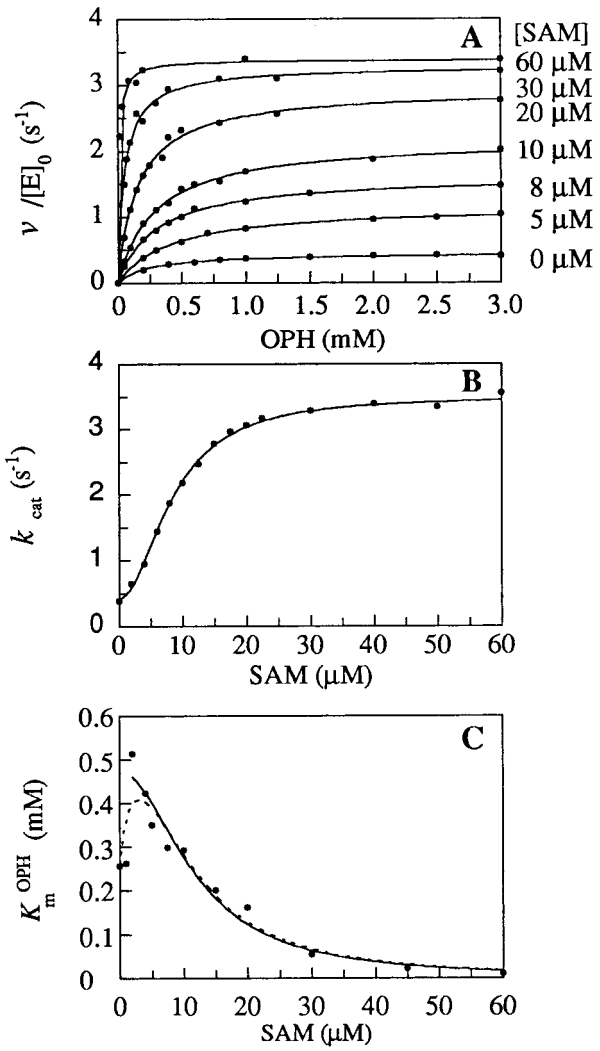

FIGURE 4: Dependence of threonine synthase activity on the concentration of OPH substrate and SAM activator. The assays contained 0.08−0.2 μM subunit of recombinant threonine synthase overexpressed in *E. coli* in a total volume of 100 μL. Reaction was initiated by addition of the purified enzyme. (A) Velocity plots. The steady-state rate of threonine synthesis ($v/[E]_0$) was measured by varying OPH concentrations for fixed SAM concentrations as indicated on the right of the plot. The points are experimental. The curves are the best fits obtained by nonlinear regression analysis of the experimental data to eq 1 (Michaelis−Menten equation). For each curve, the best fit parameter K_m^{OPH} (eq 1) was calculated. For the clarity of the figure, curves obtained for 1, 2, and 4 μM [SAM] were not indicated. (B) Plot of k_{cat} versus [SAM] determined at saturating (5 mM) concentration of OPH. The points are experimental. Curve is the best fit obtained by nonlinear regression analysis of the experimental data to eq 5 (see Discussion) for the following parameter values: $K_1K_2 = (72.6 \pm 4.2)$ μM^2, $k_{cat}^A = (0.42 \pm 0.04)$ s^{-1}, $k_{cat}^{AS2} = (3.5 \pm 0.03)$ s^{-1}. (C) Plot of K_m^{OPH} versus [SAM]. The points are experimental, and the curves were generated by curve-fitting analysis of the data corresponding to the 2−60 μM SAM concentration range [bold line; eq 9, $K_A = (474 \pm 26)$ μM and $K_1K_2 = (140 \pm 30)$ μM^2] and the whole SAM concentration range [dotted line; eq 10, $K_A = (248 \pm 18$ μM), $K_1 = (1.09 \pm 0.22)$ μM, $K'_1 = (0.5 \pm 0.06)$ μM, and $K_2 = (130 \pm 64$ μM), see Discussion] (see Figure 8 for nomenclature).

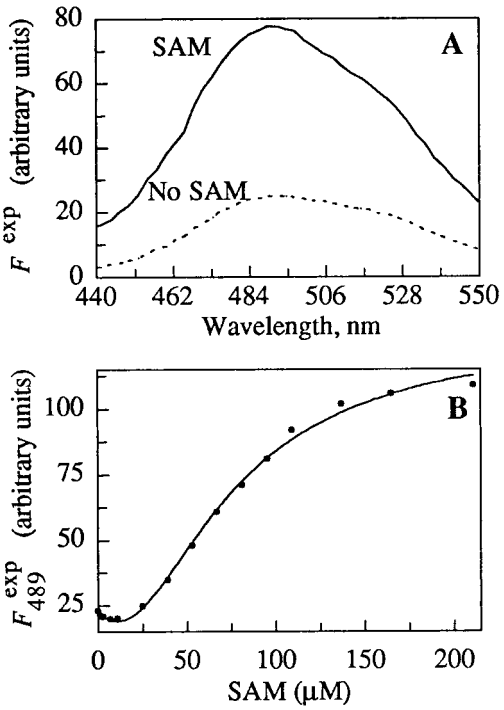

FIGURE 5: Effect of SAM on the fluorescence of threonine synthase-bound pyridoxal phosphate. (A) Fluorescence emission spectrum of threonine synthase in 50 mM Na−Hepes, pH 8.0, and 150 mM NaCl was measured upon excitation at 410 nm in the absence or the presence of 200 μM SAM. (B) Equilibrium binding of SAM to threonine synthase. The relative fluorescence change (emission monitored at 489 nm) for the enzyme (2 μM subunit) is plotted versus total [SAM]. The curve is the best fit obtained by nonlinear regression analysis of the experimental data to eq 11. The curve presented in Figure 5B fitted by this equation yielded $K'_1K'_2 = (3826 \pm 510)\ \mu M^2$, $F_0 = (22.6 \pm 1)$, $\alpha = (-0.65 \pm 0.18)$, and $\beta = (0.028 \pm 0.004)$. (See Figure 8 for nomenclature).

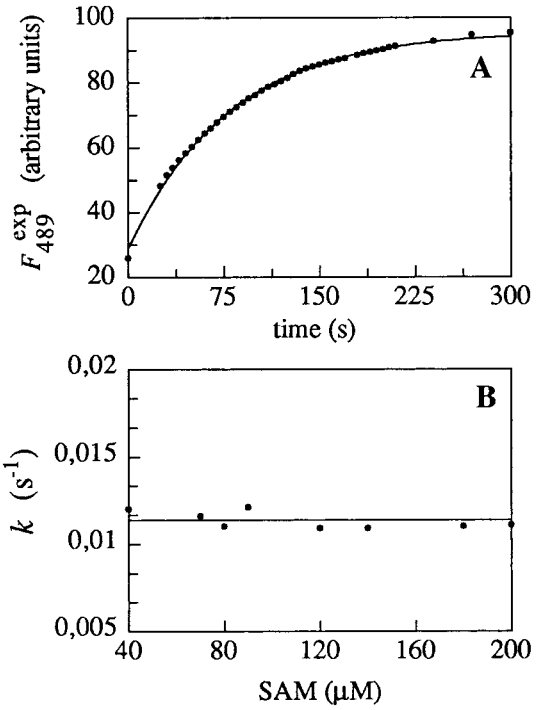

FIGURE 6: Kinetics of SAM binding to free threonine synthase as monitored by fluorescence. (A) The rate of fluorescence increase (489 nm) was measured upon the addition of 200 μM SAM (final concentration) to the free enzyme. The curve is the best fit obtained by nonlinear regression analysis of the experimental data to eq 2. (B) Effect of the SAM concentration on the time constant (k) for the 489 nm fluorescence signal increase. This time constant does not show a ligand concentration dependence, and a constant value of 0.012 s^{-1} was determined for k.

decreased and thus could not be accurately determined. For example, at 90 μM SAM, $K_m^{OPH} \leq 2\ \mu$M.

The sigmoidicity of the k_{cat} versus [SAM] curve was indicative of kinetic positive cooperativity with respect to the activator. However, a kinetic sigmoidal response to SAM is not necessarily the sign of true cooperativity. For example, sigmoidal response can arise in substrate plus effector reactions in which there is a preferred, but not exclusive, kinetic pathway to a ternary complex (*22*). Another possibility would be that SAM binding to the enzyme is slow compared to k_{cat} so that at steady state there will be a flux between catalytically different forms (the free enzyme and the SAM-bound enzyme) as occurs in hysteretic (*23*) and mnemonic (*24*) enzymes. To distinguish between these possibilities it was therefore of importance to investigate directly the mechanism of SAM association to the enzyme in equilibrium binding experiments.

Analysis of SAM Binding to the Free Enzyme by Fluorescence. To analyze more directly the association of SAM with the enzyme in the absence of OPH, we took advantage of the fluorescence properties of the protein-bound PLP cofactor. The fluorescence emission of PLP in threonine synthase underwent a large increase in the presence of SAM to the enzyme. Thus, Figure 5A shows a 4-fold increase in the fluorescence emitted at 489 nm upon addition of SAM. This observation indicates that the activator SAM can interact with the enzyme in the absence of the OPH substrate, thereby modifying the electronic environment of the PLP cofactor. When this increase in fluorescence was monitored as a function of SAM concentration, a slight decrease in the fluorescence signal was first observed at low concentrations (from 0 to 10 μM SAM) followed by a large increase obtained at SAM concentrations from 10 to 200 μM (Figure 5B).

The interaction of SAM with the free enzyme was also investigated in fluorescence kinetic experiments. Upon SAM binding to the free enzyme, the fluorescence signal (489 nm) took several minutes to reach equilibrium (Figure 6A), displaying a single observable relaxation process (eq 2)

$$F^{exp}_{489} = F_0 + \Delta F(1 - e^{-kt}) \qquad (2)$$

where F^{exp}_{489nm} represents the observed fluorescence at time t, F_0 is the initial fluorescence, ΔF is the amplitude factor, and k is the pseudo-first-order rate constant for the fluorescence signal to reach equilibrium. A plot of k versus [SAM] yielded a horizontal line (Figure 6B), suggesting that rapid binding of SAM to the enzyme was followed by an isomerization step of the SAM−enzyme complex. This isomerization was a slow phenomenon being characterized by a monomolecular rate constant of 0.012 s^{-1}, corresponding to a half-time value ($t_{1/2}$) of about 60 s.

Influence of the Concentration of OPH on Kinetic Patterns. A comparison of the SAM-saturation curves from Figures 4B (influence of SAM concentration on k_{cat}) and 5B (interaction between SAM and enzyme at equilibrium) revealed a significant difference in the $[SAM]_{0.5}$ values (the

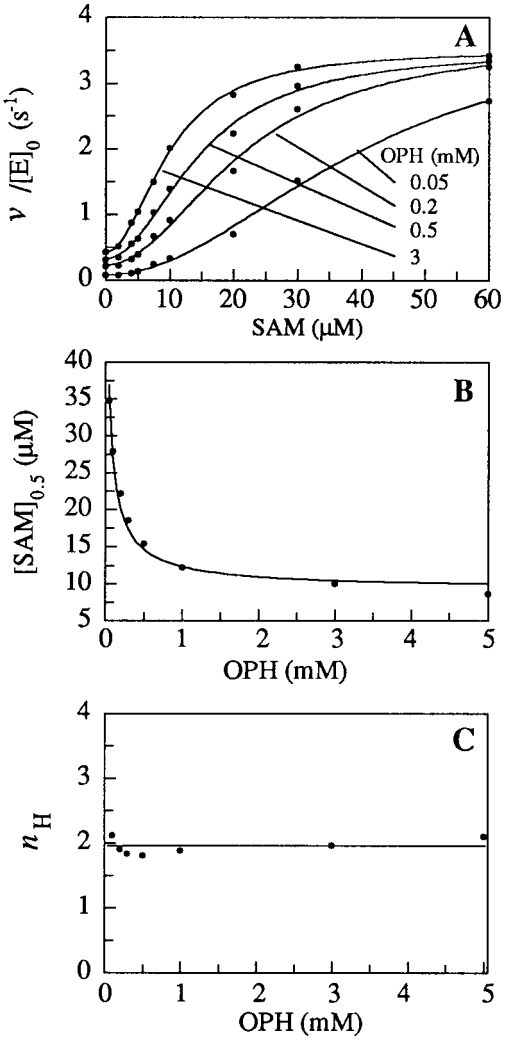

FIGURE 7: Influence of the concentration of OPH on kinetic patterns. (A) Plot of velocity versus [SAM] for different OPH concentrations. The figure is a replot of Figure 4A. The corresponding OPH concentrations are indicated. The curves are the best fits obtained by nonlinear regression analysis of the experimental data to eq 4. For the clarity of the figure, curves corresponding to 0.1, 0.3, 1, and 5 mM [OPH] were not plotted. (B) Plot of $[SAM]_{0.5}$ versus [OPH]. $[SAM]_{0.5}$ values were calculated from curves of Figure 7A fitted to the Hill equation. The curve is the best fit obtained by nonlinear regression analysis of the experimental data to eq 8 and yielded the following best fit parameters: $K_1K_2 = (88 \pm 18)\ \mu M^2$ and $K_A = (721 \pm 179)\ \mu M$. (C) Plot of Hill coefficient value (n_H) versus [OPH]. n_H values were calculated from curves of Figure 7A fitted to the Hill equation.

concentration of SAM required to reach half-maximal effect). Thus, the $[SAM]_{0.5}$ value was found to be 8 μM in the presence of 5 mM OPH (Figure 4B) and 75 μM in the absence of the substrate (Figure 5B). To determine the influence of OPH on the apparent affinity of the enzyme for SAM, the data in Figure 4A were replotted to yield SAM saturation curves at different OPH concentrations (Figure 7A). Nonlinear regression analyses of these data according to the Hill equation indicated that OPH exerted a marked effect on $[SAM]_{0.5}$ values (Figure 7B). Increasing the substrate concentration up to 5 mM was associated with a 6-fold decrease in the $[SAM]_{0.5}$ value. However, the Hill coefficient value (n_H) was not significantly affected by the presence of OPH, exhibiting a constant value close to 2 (Figure 7C).

DISCUSSION

To understand the molecular mechanism of SAM and OPH interactions with plant threonine synthase, the *A. thaliana* enzyme was overproduced in *E. coli* cells and purified to homogeneity. N-terminal sequence analysis, gel filtration experiments, and activity measurements in the presence or the absence of SAM demonstrated that the overexpressed enzyme is identical to the native enzyme isolated from leaves (*8*).

Interpretation of the Kinetic Data in Terms of a General Kinetic Model. There are two characteristic features of the reaction catalyzed by the plant threonine synthase. First, steady-state kinetic analysis clearly showed that the enzyme obeys Michaelis−Menten behavior whether it is assayed in the absence or the presence of SAM. Second, saturation isotherms of plant threonine synthase by SAM deviate from hyperbolic behavior, suggesting that at least two SAM molecules can bind on each enzyme molecule. Also, the present data established that (i) the enzyme assumes a homodimeric structure both in its native state and bound to its SAM activator and (ii) the binding of SAM and OPH to the enzyme can occur in an independent manner (the enzyme was active in the absence of SAM and the free enzyme can interact with SAM in the absence of OPH to produce characteristic spectral changes). Figure 8A depicts the simplest general kinetic model to account for these observations. To derive the steady-state rate equation, this general model can be simplified according to the following assumptions. When the SAM saturation curve corresponding to the k_{cat} data (Figure 4B) is fitted by the Hill equation, a Hill value of 2 is obtained (Figure 7C). This implies that the concentration of the intermediary, partially-SAM-saturated form (E^SA) is very low. Therefore, both conversions of E^SA to $E^S + P$ and E^SA to $E^S + A$ can be omitted. Additionnally, the direct conversion of E to E^{S2} can be omitted, due to its slow rate (Figure 6A, see later the discussion on the equilibrium binding results). Then, the simplified model shown in Figure 8B is obtained, from which the steady-state rate velocity can be written as eq 3

$$\frac{V}{[E]_0} = \frac{k^A_{cat} + k^{AS2}_{cat}\dfrac{S^2}{K_1K_2}}{\dfrac{1}{A}\left(K_A + K_{AS2}\dfrac{S^2}{K_1K_2}\right) + 1 + \dfrac{S}{K_1} + \dfrac{S^2}{K_1K_2}} \quad (3)$$

where $K_A = (k_2 + k^A_{cat})/k_1$, $K_{AS2} = (k_{14} + k^{AS2}_{cat})/k_{13}$, $K_1 = k_4/k_3$, $K_2 = k_{10}/k_9$, K^A_{cat}, and k^{AS2}_{cat} are the catalytic constants of the SAM-free and fully-SAM-saturated enzyme forms, respectively. Under the above assumption that the E^SA complex concentration is very low, then $S/K_1 \ll S^2/K_1K_2$, and eq 3 reduces to eq 4

$$\frac{V}{[E]_0} = \frac{k^A_{cat} + k^{AS2}_{cat}\dfrac{S^2}{K_1K_2}}{\dfrac{S^2}{K_1K_2}\left(\dfrac{K_{AS2}}{A} + 1\right) + \left(\dfrac{K_A}{A} + 1\right)} \quad (4)$$

from which the associated apparent k_{cat}, $[SAM]_{0.5}$, and K_m expressions take the following forms:

$$\text{apparent } k_{cat} = \frac{k^{A}_{cat} + k^{AS2}_{cat}\dfrac{S^2}{K_1K_2}}{1 + \dfrac{S^2}{K_1K_2}} \quad (5)$$

$$[\text{SAM}]_{0.5} = \left[\frac{K_1K_2\left(\dfrac{K_A}{A} + 1\right)}{\dfrac{K_{AS2}}{A} + 1}\right]^{1/2} \quad (6)$$

$$\text{apparent } K_m = \frac{K_A + K_{AS2}\dfrac{S^2}{K_1K_2}}{1 + \dfrac{S^2}{K_1K_2}} \quad (7)$$

As Figure 4B shows, a satisfactory fit was obtained by nonlinear regression analysis of the k_{cat} versus [SAM] data using eq 5 for the best fit parameter values listed in the legend to Figure 4B. Attempts to fit the K_m^{OPH} versus [SAM] data (above 2 μM SAM) using eq 7 were unsuccessful because the K_{AS2} value was largely undetermined [(4 $\pm$ 27) μM]. Setting constant the K_1K_2 value as determined in Figure 4B [i.e., $K_1K_2 = (72.6 \pm 4.2)$ μM^2] decreases the number of fitting variables from 3 to 2 in eqs 6 and 7. However, under these conditions, the K_{AS2} value was found to be (29 $\pm$ 5) μM from eq 6 and (37 $\pm$ 19) μM from eq 7. These high values are not in accordance with experimentally determined K_{AS2} since we observed that $K_{AS2} = 10$ μM at 60 μM SAM and $K_{AS2} \leq 2$ μM at 90 μM SAM. Therefore, the experimental evidence strongly suggests that K_{AS2} is very small (i.e., ≤ 1 μM). Accordingly, eqs 6 and 7 reduce to

$$[\text{SAM}]_{0.5} = \left[K_1K_2\left(\frac{K_A}{A} + 1\right)\right]^{1/2} \quad (8)$$

$$\text{apparent } K_m = K_A\left(1 + \frac{S^2}{K_1K_2}\right) \quad (9)$$

Satisfactory fit was obtained by nonlinear regression analysis of the $[\text{SAM}]_{0.5}$ versus [OPH] data using eq 8 for the best fit parameters listed in the legend to Figure 7B. In particular, the K_1K_2 value, (88 $\pm$ 18) μM^2, is close to that estimated from eq 5 [$K_1K_2 = (72.6 \pm 4.2)$ μM^2].

A more complex situation was observed for the K_m data. Since from eqs 7 or 9 the sign of the first partial derivative $dK_m^{OPH}/d[S]$ is always negative, these equations cannot fit the entire data shown in Figure 4C, particularly the sharp increase in K_m^{OPH} observed at low SAM concentrations. However, eq 9 fitted well the K_m data in the SAM concentration range from 2 to 60 μM for the best fit parameters listed in the legend of Figure 4C. We have attempted to account for the peculiar behavior seen in the low SAM concentration range (0$-$2 μM) by considering the possibility that SAM can bind to the free enzyme competitively, thus preventing binding of OPH to the enzyme and setting up an alternative pathway for binding of the enzyme

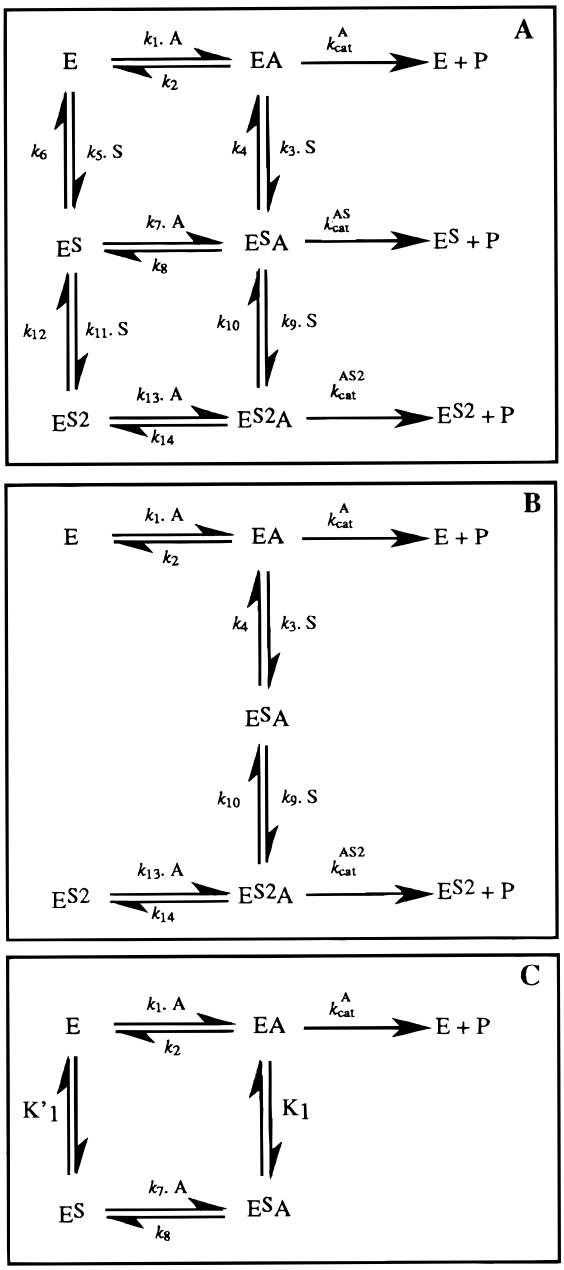

FIGURE 8: Kinetic models to account for the data. (A) General kinetic model. The model is constructed on the basis that the enzyme steady-state kinetics exhibit Michaelis$-$Menten behavior with respect to OPH substrate (either in the presence or absence of SAM; see Figure 4A) and involve binding of two SAM molecules to the enzyme (see Figure 4B). Nomenclature: E, free enzyme; A, OPH substrate; S, SAM activator; E^SA, partially-SAM-saturated enzyme$-$OPH complex; $E^{S2}A$, fully-SAM-saturated enzyme$-$OPH complex; $K_A = (k_2 + k^A_{cat})/k_1$, $K_{AS2} = (k_{14} + k^{AS2}_{cat})/k_{13}$, $K_1 = k_4/k_3$, $K'_1 = k_6/k_5$, $K_2 = k_{10}/k_9$, $K'_2 = k_{12}/k_{11}$, k^A_{cat}, and k^{AS2}_{cat} are the catalytic constants of the SAM-free and fully-SAM-saturated enzyme forms, respectively. (B) Simplified kinetic model. (C) An alternative pathway to account for the K_m^{OPH} versus [SAM] data observed in the 0$-$2 μM SAM concentration range.

substrate (Figure 8C). This competition can be taken into account, and eq 9 must be corrected to give more appropriate values when [SAM] tends to 0 by replacing K_A with an apparent K_m which is a function of [SAM]. This model can then be examined under two different assumptions. In the first, which assumes rapid equilibrium between the enzyme (E) and SAM-bound complex (E^SA), K_A must be replaced

by $K_A[(1 + S/K'_1)/(1 + S/K_1)]$, which yields eq 10

$$\text{apparent } K_m = K_A[(1 + S/K'_1)/(1 + S/K_1)]/(1 + S^2/K_1K_2) \quad (10)$$

where K'_1 and K_1 are the dissociation constants for the binding of the first SAM molecule to the free E and OPH-bound EA forms, respectively (Figure 8C). Good fit was obtained by nonlinear regression analysis of the whole K_m versus [SAM] data using eq 10 (Figure 4C). However, values of K_1 [(1.09 ± 0.22) μM], K'_1 [(0.5 ± 0.06) μM], and K_2 [(130 ± 64 μM)] parameters obtained from this curve-fitting analysis were not compatible with the observed positive kinetic cooperativity (Figure 4B). Therefore, the model in Figure 8C cannot account for the observed kinetic behavior of the enzyme under a rapid-equilibrium assumption. Alternatively, if steady-state conditions hold, then K_A must be replaced with an apparent K_m which is a complex ratio of polynomia containing $[SAM]^2$ and [SAM] terms. Furthermore, in this expression of the apparent K_m, constant terms are groupings of all rate constants in the mechanism shown in Figure 8C. Thus, the simplified model of Figure 8B modified according to Figure 8C potentially accounts for the observed data under a steady-state assumption. Unfortunately, its associated rate equation contains too many terms and therefore cannot be used to deduce explicitely the numerical value of the kinetic constants in Figure 8C by curve-fitting analysis (*25*).

In summary, the simplified kinetic model of Figure 8B can account for all the observed kinetic data, at least for SAM concentrations above 2 μM. From the results, in Figure 4C, the apparent K_m for the OPH substrate is much larger in the absence of SAM than in its presence. Good agreement between the experimental data and theoretical equations deduced from the model was obtained under the assumption that $K_2 \ll S$, meaning that once the enzyme has bound one SAM molecule, the binding of the second one is considerably facilitated.

The specificity constant (k_{cat}/K_m^{OPH}) can be calculated for both the free and fully-SAM-saturated forms to give a physical interpretation of the effect of SAM on the OPH binding. This parameter sets a lower limit for the bimolecular rate constant for encounter complex formation between enzyme and OPH (*26*). Specificity constants of 1500 M^{-1} s^{-1} and of 3.5 10^5 M^{-1} s^{-1} were calculated for association of OPH respectively on the SAM-free and the enzyme in the presence of 60 μM SAM. Thus, upon binding of the SAM activator, threonine synthase acquires marked different kinetic properties, allowing the OPH substrate to diffuse at a faster rate (200-fold) into the active site, to decrease the K_m for the substrate (25-fold), and to increase the catalytic efficiency (8-fold). This might have physiological consequences since the intraplastidial concentration of OPH is estimated to be on the order of 50 μM (*27*). In these conditions, in the absence of SAM, we can calculate that OPH would bind very slowly to the enzyme with a half-time value of approximately 10 s. In view of this, SAM may be considered as an "essential" activator of threonine synthase.

Equilibrium Binding of SAM to the Enzyme As Probed by Fluorescence Measurements. The above kinetic interpretation indicates that the enzyme binds two SAM molecules during catalysis. Assuming a sequential binding of SAM to the free enzyme

$$E \overset{K'_1}{\rightleftharpoons} E^S \overset{K'_2}{\rightleftharpoons} E^{S2}$$

where $K'_1 = k_6/k_5$ and $K'_2 = k_{12}/k_{11}$ are the equilibrium dissociation constants for binding of the first SAM and second SAM molecule, respectively, this binding can be described by eq 11

$$F^{exp}_{489nm} = \frac{F_0 + (\alpha\, S/K'_1) + (\beta\, S^2/K'_1K'_2)}{1 + (S/K'_1) + (S^2/K'_1K'_2)} \quad (11)$$

where F_0 is the initial fluorescence of the enzyme and α and β are groupings of equilibrium constants and intrinsic fluorescence coefficients for the two successive E^S and E^{S2} complexes. As Figure 5B shows, a good fit of the experimental data was obtained using eq 11 provided that $S/K'_1 \ll 1$. This means that the binding of the second molecule of SAM is considerably facilitated by the binding of the first one to the enzyme. Mathematical convergence was achieved for a negative α value in eq 11, indicating that the emission fluorescence at 489 nm of the intermediate E−SAM complex is smaller than that of the free enzyme. The β value in eq 11 was positive meaning that the emission fluorescence at 489 nm of the E^{S2} complex was higher than that of the E and E^S enzyme forms. Thus the E^S and E^{S2} complexes have distinct spectroscopic properties. This fit yielded a value of (3826 ± 510) μM^2 for $K'_1K'_2$. This value is 48-fold higher than the K_1K_2 value obtained for SAM binding to the enzyme in the presence of OPH [K_1K_2 = (72.6 ± 4.2) μM^2]. This finding therefore validates the assumptions used above to analyze the steady-state kinetic data according to the simplified model (Figure 8B).

In summary, the general kinetic model of Figure 8A fully accounts for both the steady-state kinetic data and the equilibrium binding data corresponding to SAM binding to the enzyme in the absence of OPH.

Interpretation of the Kinetic and Equilibrium Data in Terms of a Structural Model. The present work establishes that the enzyme exists as a dimer of identical subunits, each of which containing an active-site-bound PLP molecule. Furthermore, we have shown that the binding of SAM to the enzyme does not affect the oligomeric status of the enzyme. In the following, we shall attempt to interpret the kinetic model of Figure 8 in terms of a structural model. Since plant threonine synthase exists as an homodimer, it is reasonable to assume that each of the two subunits contains one substrate and one effector binding site (Scheme 1).

Within the dimeric enzyme the two OPH binding sites are both equivalent and independent because threonine synthase exhibits Michaelis−Menten behavior with respect to OPH substrate whatever the SAM concentration (Figure 4A). It is worth noting that this property of the plant threonine synthase with respect to its substrate is a rare feature for an allosteric enzyme because most of them display sigmoidal substrate saturation curves, with effectors increasing or decreasing the cooperativity for the substrate.

Though OPH and SAM appear to bind in an independent manner to the enzyme, there must exist, however, an

Scheme 1: Working Model To Account for the Interactions between SAM Activator and OPH Substrate Binding Sites in the Dimeric Threonine Synthase (See Text)

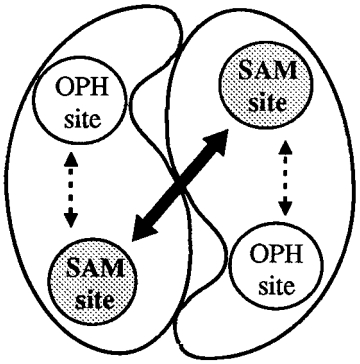

interaction between the OPH and SAM binding sites within each subunit. Indeed, the large modifications of the active-site-bound PLP fluorescence signal upon SAM binding attest that SAM modifies in some way the electronic environment of the enzyme active sites. Reciprocally, OPH binding to the enzyme was shown to decrease about 6-fold the $[SAM]_{0.5}$ value, meaning that occupancy of the OPH binding sites led to an increased affinity for binding the activator. This potential interaction between the SAM and OPH binding sites is depicted by the small dashed arrow in Scheme 1.

The results of equilibrium binding experiments indicated that the binding of one SAM molecule to one of the two enzyme subunits facilitates the binding of the second SAM molecule. In other words, there exists a positive interaction between the two SAM binding sites (Scheme 1, bold arrow). In agreement with this finding, from steady-state measurements, a Hill coefficient value close to 2 can be calculated when SAM saturation curves (Figure 7A,C) are fitted to the Hill equation. Since such a value represents the maximal value that can be obtained for a dimeric enzyme both subunits are strongly constrained by their association, suggesting that they change their conformation upon SAM binding in a concerted manner. However, the observed decrease in fluorescence at 489 nm detected in the low SAM concentration range (Figure 5B) suggests the existence of a partially-SAM-saturated enzyme form that is characterized by spectroscopic properties different from those of the free and fully-SAM-saturated enzyme forms. Such an observation is in favor of a sequential model (*28*) of SAM binding to the enzyme, at least in the absence of OPH.

A kinetic analysis of the modification of enzyme-bound PLP fluorescence spectrum induced by SAM binding at high concentrations (above 40 μM) showed a single monophasic process, for which the time constant was found to be independent of the SAM concentration. We interpret these data as showing that binding of the second molecule of SAM to the E^SA intermediate occurs in at least two steps: a fast bimolecular step of encounter complex formation (not observable in our experiments) and a slower monomolecular step of rearrangement of the encounter complex ($t_{1/2}$ = 60 s). When SAM is removed by dialysis from an enzyme−SAM solution, the enzyme fluorescence spectrum returns to that of the free enzyme, thus indicating that the whole process is reversible (data not shown). Kinetics of the modification of the enzyme-bound PLP fluorescence in the simultaneous presence of SAM (100 μM) and OPH (250 μM) were monitored in preliminary stopped-flow experiments (not shown). We observed an increase in the fluorescence signal at 489 nm that occurs at a much faster rate ($t_{1/2}$ = 3.2 s) than that seen in the absence of OPH. We suggest, therefore, that the monomolecular step of the E^{S2} encounter complex rearrangement corresponds to an allosteric transition as described in the initial nomenclature of Monod, Changeux, and Jacob (*29*), though it applies here to the activator rather than to the substrate. Furthermore, our results strongly suggest that OPH binding facilitates such an allosteric transition induced by SAM. However, it does so without affecting the interactions between the two subunits since the Hill value, n_H, remains constant as a function of OPH concentration (Figure 7C).

As inferred from calculation of the specificity constants for OPH in the absence or presence of SAM (see above) the consequence of the allosteric transition on the association between the enzyme and OPH is to increase dramatically, by 200-fold, the bimolecular rate constant for OPH binding to the enzyme. This suggests a more "open" conformation of the substrate binding site in the SAM-saturated enzyme compared to the free enzyme.

Our working model remains to be clarified with respect to the exact stoichiometry SAM/subunit, and further experiments using site-directed mutagenesis are in progress to answer this question.

ACKNOWLEDGMENT

The contribution of one of the referees of this paper to the kinetic analysis is deeply acknowledged. We also acknowledge Dr. D. Faucher and A. Breton Gilet (Rhône-Poulenc Rorer, Vitry-Alfortville, France) for the amino acid sequencing. We are grateful to Dr. S. Ravanel for help in the PLP-bound peptide purification, to D. Just and J. L. Guesnet in the NMR analyses of *O*-phosphohomoserine preparation, and to Dr. M. Desmadril in the stopped-flow kinetic analyses. We thank Dr. A. Cornish-Bowden, Dr. R. DeRose, and Dr. G. Hervé for helpful discussions.

REFERENCES

1. Singh, B. K., and Shaner, D. L. (1995) *Plant Cell 7*, 935−944.
2. Galili, G., Karchi, H., Shaul, O., Perl, A., Cahana, A., Tzchori, B. T., Zhu, X. Z., and Galili, S. (1994) *Transgen. Plants Plant Biochem. 22*, 921−925.
3. Madison, J. T., and Thompson, J. F. (1976) *Biochem. Biophys. Res. Com. 71*, 684−691.
4. Giovanelli, J., Veluthambi, K., Thompson, G. A., Mudd, S. H., and Datko, A. H. (1984) *Plant Physiol. 76*, 285−292.
5. Kreft, B. D., Townsend, A., Pohlenz, H. D., and Laber, B. (1994) *Plant Physiol. 104*, 1215−1220.
6. Aarnes, H. (1978) *Planta 140*, 185−192.
7. Thoen, A., Rognes, S. E., and Aarnes, H. (1978) *Plant Sci. Lett. 13*, 113−119.
8. Curien, G., Dumas, R., Ravanel, S., and Douce, R. (1996) *FEBS Lett. 390*, 85−90.
9. Umbarger, H. E. (1978) *Annu. Rev. Biochem. 47*, 533−606.
10. Roper, M. D., and Kraus, J. P. (1992) *Arch. Biochem. Biophys. 298*, 514−521.
11. Ravanel, S., Droux, M., and Douce, R. (1995) *Arch. Biochem. Biophys. 316*, 572−584.
12. Lanzetta, P. A., Alvarez, L. J., Reinach, P. S., and Candia, O. A. (1979) *Anal. Biochem. 100*, 95−97.

13. Glazer, R. I., and Peale, A. L. (1978) *Anal. Biochem. 91*, 516−520.
14. Shapiro, S. K., and Ehninger, D. J. (1966) *Anal. Biochem. 15*, 323.
15. Lewin, L. M., and Brown, G. M. (1963) *Arch. Biochem. Biophys. 101*, 197−203.
16. Rolland, N., Ruffet, M. L., Job, D., Douce, R., Droux, M. (1996) *Eur. J. Biochem. 236*, 272−282.
17. Chua, N. H. (1980) *Methods Enzymol. 69*, 434−436.
18. Bradford, M. M. (1976) *Anal. Biochem. 72*, 248−254.
19. Scopes, R. K. (1974) *Anal. Biochem. 59*, 277−282.
20. Leussing, D. A. (1986) in *Vitamin B6, Pyridoxal phosphate* (Dolphin, D., Poulson, R., and Avramovic, O., Eds.) Part A, pp 69−115, Wiley-Interscience, New York.
21. Laber, B., Gerbling, K. P., Harde, C., Neff, K. H., Nordhoff, E., and Pohlenz, H. D. (1994) *Biochemistry 33*, 3413−3423.
22. Ferdinand, W. (1966) *Biochem. J. 98*, 278−283.
23. Neet, K. E., and Ainslie, G. R. (1980) *Methods Enzymol. 64B*, 192−226.
24. Meunier, J. C., Buc, J., Navarro, A., and Ricard, J. (1974) *Eur. J. Biochem. 49*, 209−223.
25. Segel, I. H. (1975) in *Enzymes Kinetics: Behavior and Analysis of Rapid Equilibrium and Steady-State Enzyme Systems*, pp 198−202, John Wiley and Sons, New York.
26. Fersht, A. (1985) in *Enzyme Structure and Mechanisms*, 2nd ed., pp 98−154, Freeman, W. H. Co., New York.
27. Giovanelli, J., Mudd, S. H., Datko, A. H., and Thompson, G. A. (1986) *Plant Physiol. 81*, 577−583.
28. Koshland, D. E., Némethy, G., and Filmer, D. (1966) *Biochemistry 5*, 365−385.
29. Monod, J., Changeux, J. P., and Jacob, F. (1963) *J. Mol. Biol. 6*, 306−329.

BI980068F